Max-Planck-Institut
für Meteorologie

REPORT No. 70

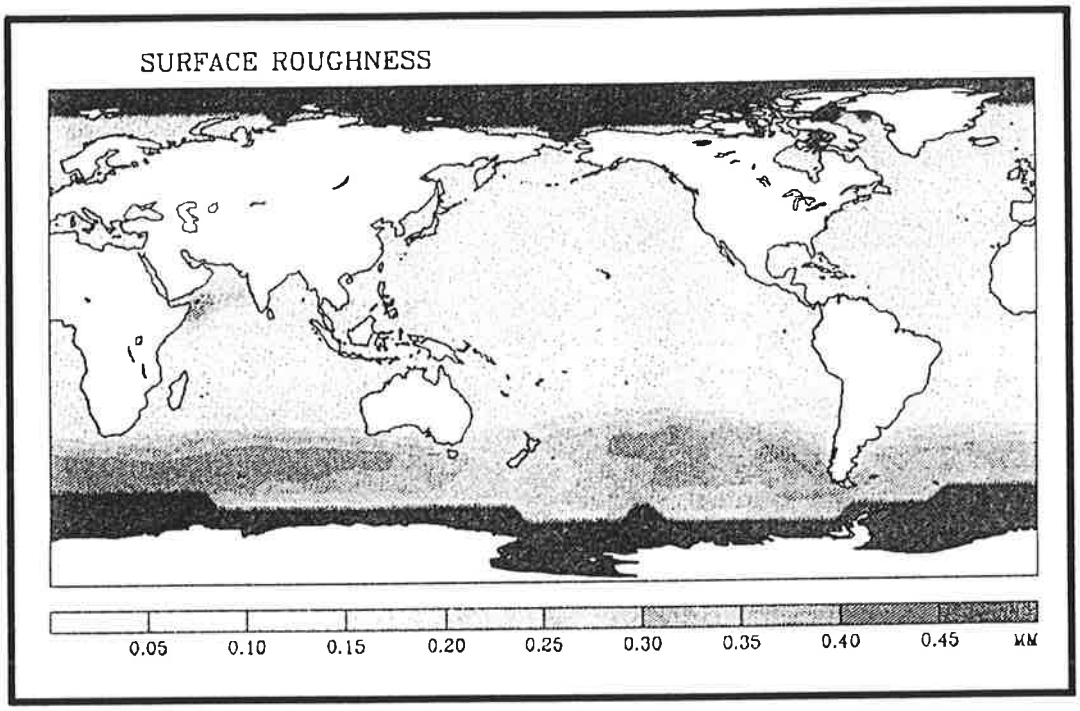

THE EFFECT OF A REGIONAL INCREASE IN OCEAN SURFACE ROUGHNESS ON THE TROPOSPHERIC CIRCULATION: A GCM EXPERIMENT

by

UWE ULBRICH • GERD BÜRGER • DIERK SCHRIEVER
HANS VON STORCH • SUSANNE L. WEBER • GERHARD SCHMITZ

HAMBURG, SEPTEMBER 1991

AUTHORS:

UWE ULBRICH

INSTITUT FÜR GEOPHYSIK UND METEOROLOGIE
ALBERTUS-MAGNUS-PLATZ
KERPENER STR. 13
5000 KÖLN 41
GERMANY

GERD BÜRGER
DIERK SCHRIEVER
HANS VON STORCH

MAX-PLANCK-INSTITUT
FÜR METEOROLOGIE

SUSANNE WEBER

KONINKLIJK NEDERLANDS
METEOROLOGISCH INSTITUUT
POST BOX 201
3730. AE DE BILT
NETHERLANDS

GERHARD SCHMITZ

OBSERVATORIUM FÜR
ATMOSPHÄRENFORSCHUNG
SCHLOSS-STR. 4-6
O-2565 KÜHLUNGSBORN
GERMANY

MAX-PLANCK-INSTITUT
FUER METEOROLOGIE
BUNDESSTRASSE 55
D-2000 HAMBURG 13
F.R. GERMANY

Tel.: +49 (40) 4 11 73-0
Telex: 211092 mpime d
Telemail: MPI.METEOROLOGY
Telefax: +49 (40) 4 11 73-298

The Effect of a Regional Increase in Ocean Surface Roughness on the Tropospheric Circulation: A GCM Experiment

Uwe Ulbrich
Institut für Geophysik und Meteorologie, Köln, Germany

Gerd Bürger, Dierk Schriever and Hans von Storch
Max Planck Institut für Meteorologie, Hamburg, Germany

Susanne L. Weber
Koninklijk Nederlands Meteorologisch Instituut, De Bilt, The Netherlands

Gerhard Schmitz
Observatorium für Atmosphärenforschung, Kühlungsborn, Germany

Abstract

The effect of an increased ocean surface roughness in the Southern Hemisphere storm track is investigated in a paired General Circulation Model sensitivity experiment. Two extended runs under permanent-July conditions are made. One with standard surface roughness, the other with a tenfold surface roughness over open sea poleward of 40°S.

The regionally enhanced ocean surface roughness modifies the tropospheric circulation in the Southern Hemisphere. The strongest effect is the reduction of tropospheric winds above the area with increased roughness. This signal is not balanced by a changed meridional temperature gradient in the lower atmosphere, but by a shift of atmospheric mass towards the Antarctic. There is a small reduction of vertical stability. The poleward eddy momentum flux is reduced in the upper troposphere and the meridional eddy sensible heat flux is reduced in the lower troposphere. Zonal mean and eddy kinetic energy are consistently reduced.

ISSN 0937–1060

1. INTRODUCTION

Surface fluxes of momentum and heat are important processes in the parameterization package of a general circulation model (GCM). A characteristic parameter in the parameterization of these fluxes is the surface roughness length or, equivalently, the neutral drag coefficient. It is not clear whether the model circulation is sensitive to variations of these parameters. A global doubling of the roughness length has little impact on the atmospheric circulation (Miller et al., 1989)

A regional instead of a global modification of the surface roughness may have a significant impact on the atmospheric circulation. Kitoh and Yamazaki (1991) and Sud and Smith (1985) indeed found a stronger atmospheric circulation in the tropics, related to enhanced latent heat fluxes, as a response to increased roughness in the tropics.

In primitive equation models the atmospheric circulation is sensitive to changes in the surface fluxes. James and Gray (1986) found that increasing the drag coefficient by a factor of ten and more induces lower zonal and higher eddy energies. On the other hand, Branscome et al. (1989) found a reduction of all energy reservoirs as a response to the inclusion of surface fluxes in their model.

In the present study we investigate whether an increase of ocean surface roughness in the Southern Hemisphere storm track does effect the atmospheric circulation. Our original motivation was related to the interaction of ocean surface waves with the atmospheric boundary layer. The surface momentum flux is known to be enhanced directly after a sudden change in the surface winds, due to the generation of waves on the ocean surface (Donelan, 1982; Maat et al., 1991; Janssen, 1989). Thus the wave field is a sink of momentum for the boundary layer, which can possibly be parameterized by an increase of the roughness length in the storm tracks. Therefore we enhanced in an idealized sensitivity experiment the surface roughness uniformly poleward of 40°S. In the present paper we compare the circulation, modified by the enhanced roughness, with that obtained in a control run. In the Discussion we come back to the question if our experimental set-up is adequate to describe the effect of ocean wave generation by abruptly changing surface winds.

The design of the GCM experiment and the statistical techniques employed are described in Section 2. In Section 3 the results of the experiment are presented: first the statistical stability of the signal is investigated; then the effect of the regionally enhanced surface roughness on the time-mean fields and on the eddy fields is discussed; finally the impact on the atmospheric energy cycle is studied. In Section 4 the paper is concluded with a discussion of the dynamic processes involved and of the significance of our experiment for the parameterization of the momentum flux from the atmospheric flow to the ocean wave field.

2. Technical Preliminaries

a) The GCM runs

We use a low resolution GCM, called ECHAM1, which is a modified version of the ECMWF operational numerical weather prediction model adapted for climate simulation purposes (Roeckner et al., 1989). The horizontal grid, on which surface processes are calculated, is a 64 longitude × 32 Gaussian latitude grid. The vertical discretization consists of 19 unevenly distributed hybrid levels.

The roughness length z_o of the ocean surface is given in the GCM by the Charnock (1955) formula, modified by a minimum condition:

$$z_o = \max \left[\alpha \frac{\tau}{g\rho}; 0.15 \text{ mm} \right]$$

where τ is the magnitude of the turbulent surface stress, g is the gravitational constant, ρ is the density of air and α is a tunable proportionality constant. The minimum roughness represents the limit of viscous flow. For a neutral stratification the roughness length is related to the drag coefficient c_D at height z by:

$$c_D(z) = \left(0.4/\ln (z/z_o)\right)^2$$

In the case of a nonneutral atmosphere this coefficient is modified with a factor which depends on the Richardson number.

Two experiments were performed: one with the standard α = 0.018 everywhere, and the other with the same α = 0.018 north of 40°S and the tenfold α = 0.18 over the open ocean south of 40°S. Both runs were made under "permanent-July" conditions. Such a model run without an annual cycle yields a comparatively large number of samples. The Southern Winter month is chosen because maximum surface wind variability is observed over the Southern Ocean at that time (Trenberth and Olson, 1988). Both runs were integrated over 24 months. The first 4 months of the control run and of the experimental run are not used in the analysis in order to exclude possible effects of initial values.

The time-mean difference between the roughness in the experiment and the roughness in the control run is shown in Fig 1. In the area where α was not changed, z_o is almost unchanged. In the 40°-60°S belt z_o is enhanced by 2-3 mm. Maximum increases of 5 mm are in the Indian Ocean.

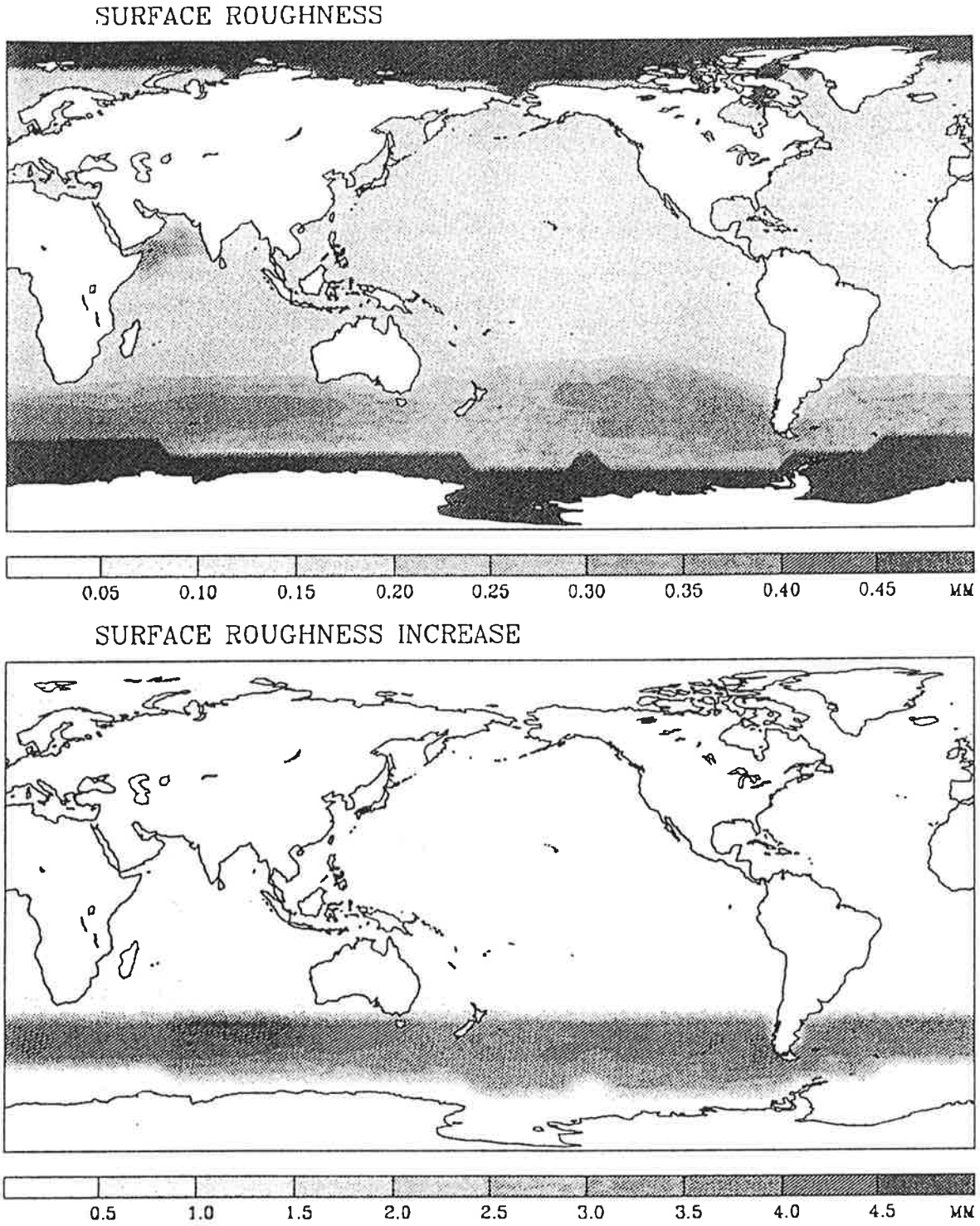

Figure 1

The global distribution of ocean surface roughness (in mm) in the ECHAM atmospheric GCM:

Top: the time-mean field in the control run,

Bottom: the difference "experiment minus control".

b) Statistics

A prerequisite for any *physical* discussion is the existence of a statistically significant signal in the simulated data, i.e., the certainty that the differences between the two runs are due to the experimental change and that they do not reflect random fluctuations.

Hasselmann (1979) proposed a general procedure to identify a statistically significant signal in a noisy, multidimensional environment. The procedure was shown to be useful by, among others, Hannoschöck and Frankignoul (1985), Storch (1987) and Hense et al. (1990). Its general idea is to project the raw data onto a low-dimensional space which contains, hopefully, the signal. The selection of this low-dimensional space may be done in a hierarchical manner such that the significance and the statistical stability of the signal are optimized. In the second step of the procedure a multivariate statistical test is applied to the reduced data. The fact that this is done in a low-dimensional space increases the power of the test and facilitates the detection of the signal when the signal-to-noise ratio is small. After having ascertained the reality of the signal, a further analysis of the statistical stability of the regional details of the (multidimensional) signal is often useful.

In the following we outline some aspects of the signal-detection strategy that we have used in our study in more detail. In this analysis we consider $\mathbf{x}$ and $\mathbf{y}$ which are two d dimensional vectors representing the control run and the experimental run. In the present study we use the latitude-height distribution of zonally averaged time-mean zonal wind. There are n realizations $\mathbf{x}(i)$ of $\mathbf{x}$ and m realizations $\mathbf{y}(i)$ of $\mathbf{y}$. The mean over the n (m) realizations of $\mathbf{x}$ ($\mathbf{y}$) is $\bar{\mathbf{x}}$ ($\bar{\mathbf{y}}$).

Guess patterns

In our example d is of the order 100 or more and n and m are of the order 10. We can reduce the number of degrees of freedom using *guess patterns* with dimension k, where $k \ll d$ (Hasselmann, 1979). The *a-priori* chosen patterns are expected to describe the signal as well as possible. The data are projected into this k dimensional *guess space*, where the multivariate statistical tests are performed. If there is a statistically significant signal in the low dimensional guess space, the multivariate signal itself is restored by expansion in the guess patterns. The resulting signal S_k in the full space is

called the *filtered signal.* A measure of the skill of the filtered signal is the *explained variance* of the full signal, i.e., the percentage of the variance of the full signal that is explained by the filtered signal.

The tests need not be done in only one k dimensional guess space. In the *hierarchical* mode (Barnett et al., 1981) a maximum number K of guess patterns is selected, and the test is done in the series of guess spaces spanned by the first k guess-patterns, k=1,...,K, consecutively.

There are several strategies to obtain guess-patterns (Storch, 1987; Hense et al., 1990). In the present study we use Empirical Orthogonal Functions (EOFs) and we order them according to descending eigenvalue.

The multivariate Hotelling test

The Hotelling test or multivariate t-test (e.g., Morrison, 1976) evaluates the null-hypothesis $\mu_x = \mu_y$, with μ_x and μ_y denoting the expectations of $\mathbf{x}$ and $\mathbf{y}$. One assumes that $\mathbf{x}$ and $\mathbf{y}$ are normally distributed with equal variances. The Hotelling test statistic is given by:

$$T^2 = \frac{n \cdot m}{n+m} \cdot (\bar{\mathbf{x}}-\bar{\mathbf{y}})^t \cdot \Gamma^{-1} \cdot (\bar{\mathbf{x}}-\bar{\mathbf{y}})$$

Here ^{t} denotes the transpose and Γ is the estimated pooled covariance-matrix of the test ensembles:

$$\Gamma = \frac{1}{n+m-2} \cdot \left(\sum_{i=1}^{n} (\mathbf{x}(i)-\bar{\mathbf{x}}) \cdot (\mathbf{x}(i)-\bar{\mathbf{x}})^t + \sum_{i=1}^{m} (\mathbf{y}(i)-\bar{\mathbf{y}}) \cdot (\mathbf{y}(i)-\bar{\mathbf{y}})^t \right)$$

Note that the matrix Γ is singular if $d > n+m-2$. Up to some scaling factor, T^2 is Fisher-F distributed if the null-hypothesis $\mu_x = \mu_y$ holds. Thus, we reject the null-hypothesis $\mu_x = \mu_y$ at the α-th level, or, with a *risk* of $(1-\alpha)$ if:

$$T^2 > \frac{(n+m-2) \cdot d}{n+m-d-1} \cdot F_{\alpha;d,n+m-d-1}$$

where $F_{\alpha;d,n+m-d-1}$ denotes the α-quantile of the Fisher-distribution with d and $n+m-d-1$ degrees of freedom.

If the null-hypothesis $\mu_x = \mu_y$ has been rejected, the difference $\bar{\mathbf{y}}-\bar{\mathbf{x}}$ is called the *significant signal.*

Multivariate Recurrence Analysis

A small risk of erroneously rejecting the null-hypothesis does not necessarily imply that the samples are well separated and that the signal is strong. If very many samples are available the power of a test to detect even small differences becomes large. The parameter *level of recurrence* (Zwiers and Storch, 1989) measures the discrimination between the control sample and the experimental sample. To obtain this parameter the d-dimensional space is split up into two disjoint sets Θ_x and Θ_y, so that the probabilities for any realization $\mathbf{x}$ to be in Θ_x and for any realization $\mathbf{y}$ to be in Θ_y are maximum:

$$\text{Prob}(\mathbf{x}\in\Theta_x) = \text{Prob}(\mathbf{y}\in\Theta_y) = p$$

Since Θ_x and Θ_y are disjoint the probability for any $\mathbf{x}$ to hit Θ_y or for any $\mathbf{y}$ to hit Θ_x are minimum:

$$\text{Prob}(\mathbf{y}\in\Theta_x) = \text{Prob}\ (\mathbf{x}\in\Theta_y) = 1\text{-}p$$

The larger the *level of recurrence* p is, the smaller is the overlap between the two distributions. An alterative interpretation is: if the level of recurrence is p and if $\mathbf{z}$ is drawn randomly either from $\mathbf{x}$ or from $\mathbf{y}$, then the chance to guess the origin of $\mathbf{z}$ correctly is p.

Test hierarchies

For each of the guess spaces, spanned by the first k guess patterns, the risk $(1\text{-}\alpha_k)$ of rejecting the null-hypothesis and the level of recurrence p_k are derived. That filtered signal S_k with $\alpha_k \geq 99\%$ and maximum p_k is selected as the *significant* filtered signal. Note that the number K of guess patterns has a maximum of $n+m$-3, because the estimated pooled covariance matrix Γ is singular for larger dimensional subspaces.

Serial correlation

Statistical tests, as the Hotelling test or the t-test, operate on sets of *independent and identically distributed* samples. In our experiments the GCM is integrated in the permanent-July mode so that T-day means are, apart from possible trends, identically distributed. But consecutive T-day means are *not* independent, due to serial correlation.

There are two ways of dealing with this serial correlation. One approach is to form T-day means (i.e., means taken over T consecutive days) not from adjacent T-day intervals, but to use instead intervals of length T+δ. Then the mean of

the first T days of each interval of length T+δ is calculated. Here δ is the time after which the atmospheric fields lose their memory, i.e., the time after which the auto-correlation has decreased to zero. After Gutzler and Mo (1983) and Trenberth (1985) δ = 10 days is an adequate choice. The other approach is to perform the statistical test as usual, but to use a corrected value for the number of test samples (realizations). If N is the total length of a time series, then n = N/T samples are available. The number of *independent* samples, which are contained in the total of all samples, is n^* = n·T/(T+δ) = N/(T+δ). Therefore, with N = 600 and δ = 10, we find with both approaches that the number of independent samples is 15 for T = 30 days, whereas it is 30 for T = 10 days.

Local analyses

After having identified a significant filtered signal S_k by means of the multivariate Hotelling test and the multivariate recurrence analysis in one physical quantity, we proceed with "local" analyses at each grid-point. The statistical stability of the signal in other quantities is examined locally by the t-test, using adjacent 30-day intervals and an adjusted number of test samples $n^* = m^* = 15$.

3. RESULTS

We apply the statistical framework outlined in the previous section to our GCM experiments to determine if enhancing roughness in the Southern Hemisphere storm track has significantly changed the model climate.

A zonally averaged quantity is denoted by []-brackets, whereas the deviation from the zonal mean is denoted by a prime. A "mean" refers to a time-mean and is denoted by an overbar.

a) Identification of a statistically significant signal

We consider the latitude-height distribution of the zonally averaged time-mean zonal wind, denoted by $[\bar{u}]$, taken at ten pressure levels between 1000 hPa and 20 hPa, and at seventeen Gaussian latitudes between 25°N and 65°S. We concentrate the analysis on the Southern Hemisphere because we anticipate the signal to be primarily in the Southern Hemisphere.

In a first attempt, we select the variables **x** and **y** to be *monthly* means, i.e., T = 30 days. Then, $n = m = 15$ independent samples are available. The risks $(1-\alpha_k)$ of erroneously rejecting the null-hypothesis of equal means, is larger than 20% for all $K = n+m-3 = 27$ elements in the hierarchy of guess spaces (not shown).

With T = 10 days, $n = m = 30$ independent samples are available, and the hierarchy length is $K = 57$. This choice of T leads to a marked improvement of the power of the Hotelling-test (Fig. 2). S_{30} is chosen as the significant filtered signal, because $p_{30} = 82\%$ is maximum and $\alpha_{30} > 99\%$; S_{30} explains 97% of the variance of the full signal. The filtered signal (Fig. 3) represents a weakening of the zonal mean circulation. In the troposphere there is an easterly anomaly between 40°S and 70°S and a westerly anomaly between 30°S and 10°N. The pattern is reversed in the stratosphere.

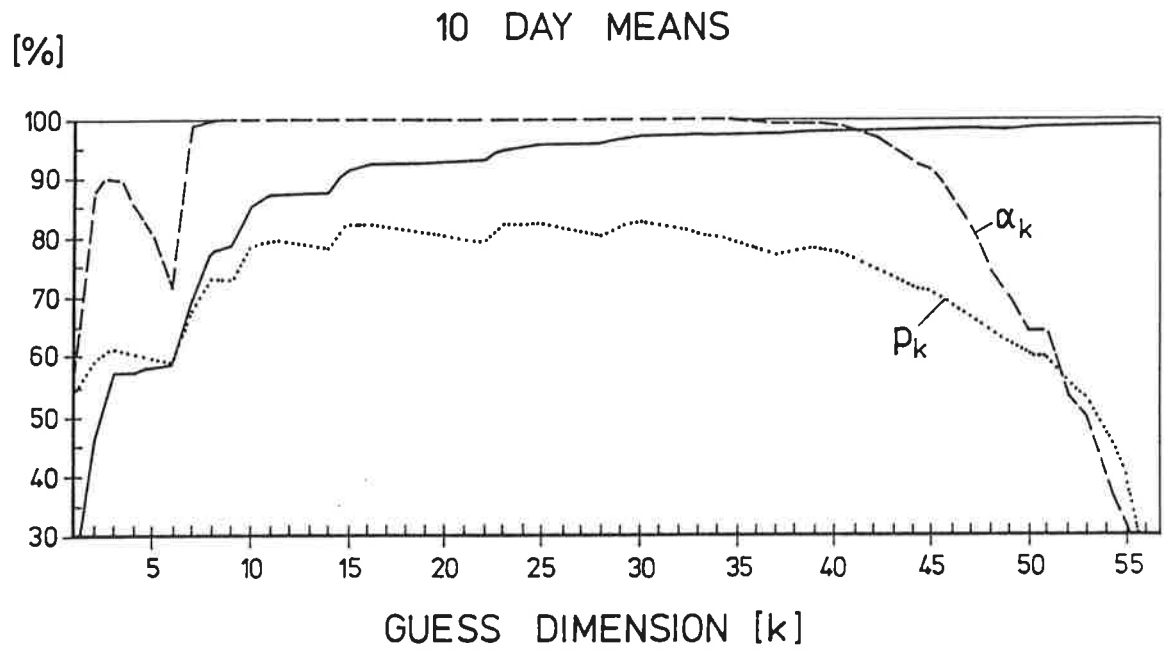

Figure 2

Multivariate analysis of the signal "experiment minus control" in the zonally averaged 10-day mean zonal wind [ū] in the Southern Hemisphere: the signal is projected onto the guess-space spanned by the first k EOFs (k=1,57) and the significance levels α_k (dashed), levels of recurrence p_k (dotted) and explained variance (solid) are computed as functions of the hierarchy parameter k.

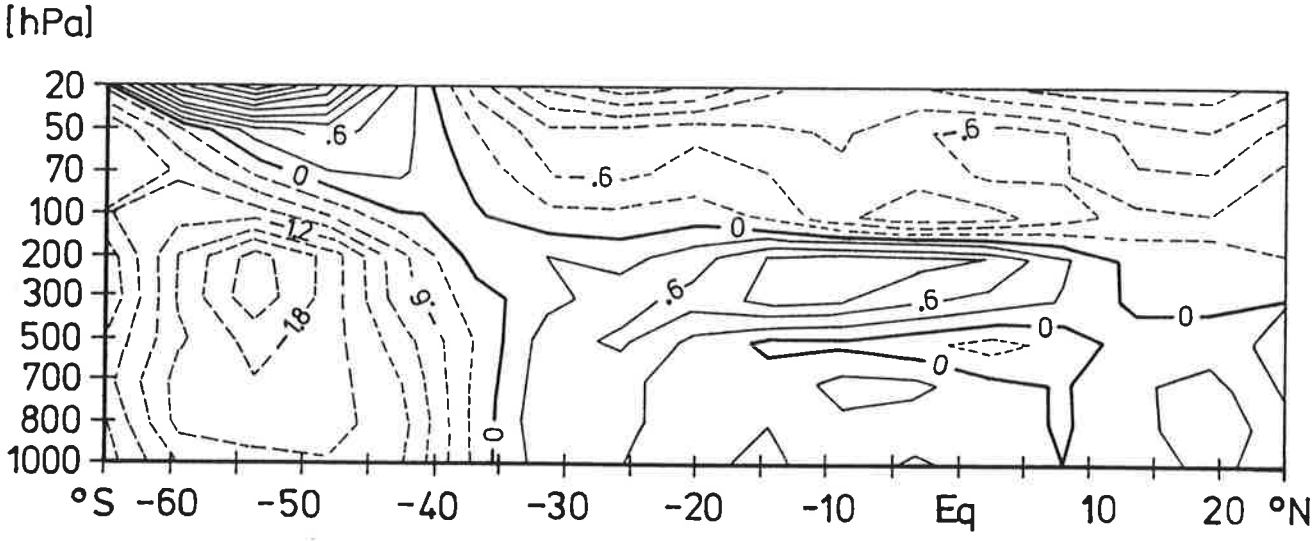

Figure 3

The significant filtered response S_{30} (experiment minus control) of the zonally averaged 10-day mean zonal wind [ū] to the enhanced ocean surface roughness south of 40° S. The risk ($1-\alpha_{30}$) that S_{30} is merely reflecting random variations is less than 1%; S_{30} is associated with a recurrence-level p_{30} of 82%

b) Local analyses of the signal

Now that the existence of a significant signal has been established, we continue our analysis with local tests of monthly mean fields.

Latitude-height distribution of zonally averaged mean fields

As expected, the full signal (experiment minus control) in the zonal wind $[\bar{u}]$ (Fig. 4a) is very similar to the filtered signal (Fig. 3). A maximum reduction in the zonal wind, by more than 2 m/s, is found in the area above the increased surface roughness. The tropospheric pattern has little vertical variations and is, according to the local *t*-test, statistically highly stable. The decrease of the zonal wind in the storm track is consistently reflected in the hemispheric mass distribution (Fig. 4b). Being in geostrophic balance, geopotential heights have increased (decreased) at all latitudes poleward (equatorward) of 40°S.

Meridional temperature contrasts in the Southern Hemisphere are only slightly altered (not shown). The temperature has increased (decreased) by about 0.5 K below (above) 500 hPa south of 30°N, which implies a reduction in the static stability. This signal is associated with slightly increased low level humidity (not shown). The vertical velocity $[\bar{\omega}]$ (Fig. 5) and the meridional velocity $[\bar{v}]$ (not shown) have slightly decreased above the regions with increased roughness. Apart from these local effects, the anomalies in $[\bar{v}]$ and in $[\bar{\omega}]$ indicate a 5% - 10% weakening of the Hadley cell. This weakening is marginally statistically stable.

Latitude-height distribution of zonally averaged eddy fields

In this Subsection we examine the eddy variance. In the Southern Hemisphere most of the eddy variance is contributed by the transient eddies.

The eddy signals in the horizontal and vertical wind components (Fig. 6a), in the geopotential height (Fig. 6b) and in the temperature are similar. The most prominent feature is the reduction of eddy intensity in the storm track and at higher levels above the Antarctic. A signal in the vertical wind, which is not observed in the other quantities, is an increase close to 20°S. This indicates an equatorward shift of the area of maximum variability in addition to the local weakening of the mean vertical wind (Fig. 5).

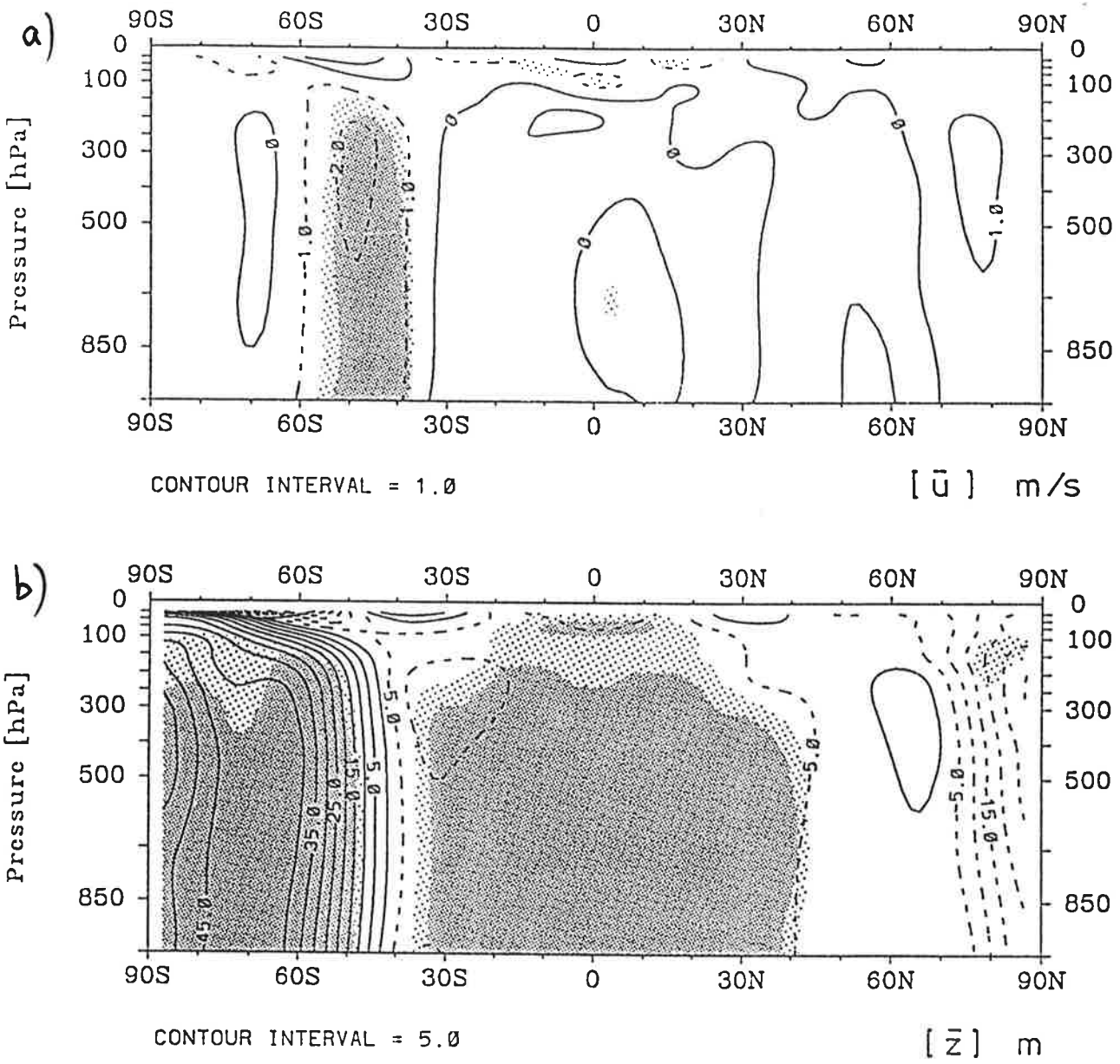

Figure 4

The latitude-height distribution of the difference "experiment - control" in the zonally averaged time-mean field of:

a) the zonal-wind ($[\bar{u}]$; units: m/s)

b) the geopotential height ($[\bar{z}]$; units: gpm)

Differences which are locally significant at the 5% (1%) level are indicated by light (heavy) shading.

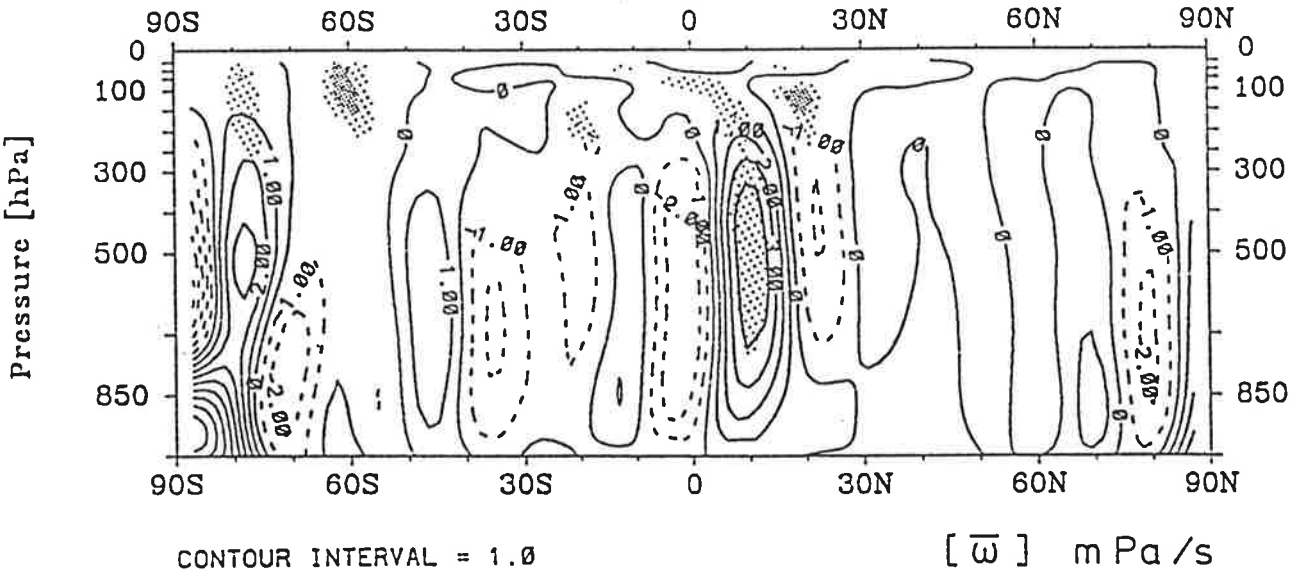

Figure 5

The latitude-height distribution of the difference "experiment - control" in the zonally averaged time-mean vertical ω-wind ([$\bar{\omega}$]; units: 10^{-3} Pa/s). Differences which are locally significant at the 5% level are indicated by light shading.

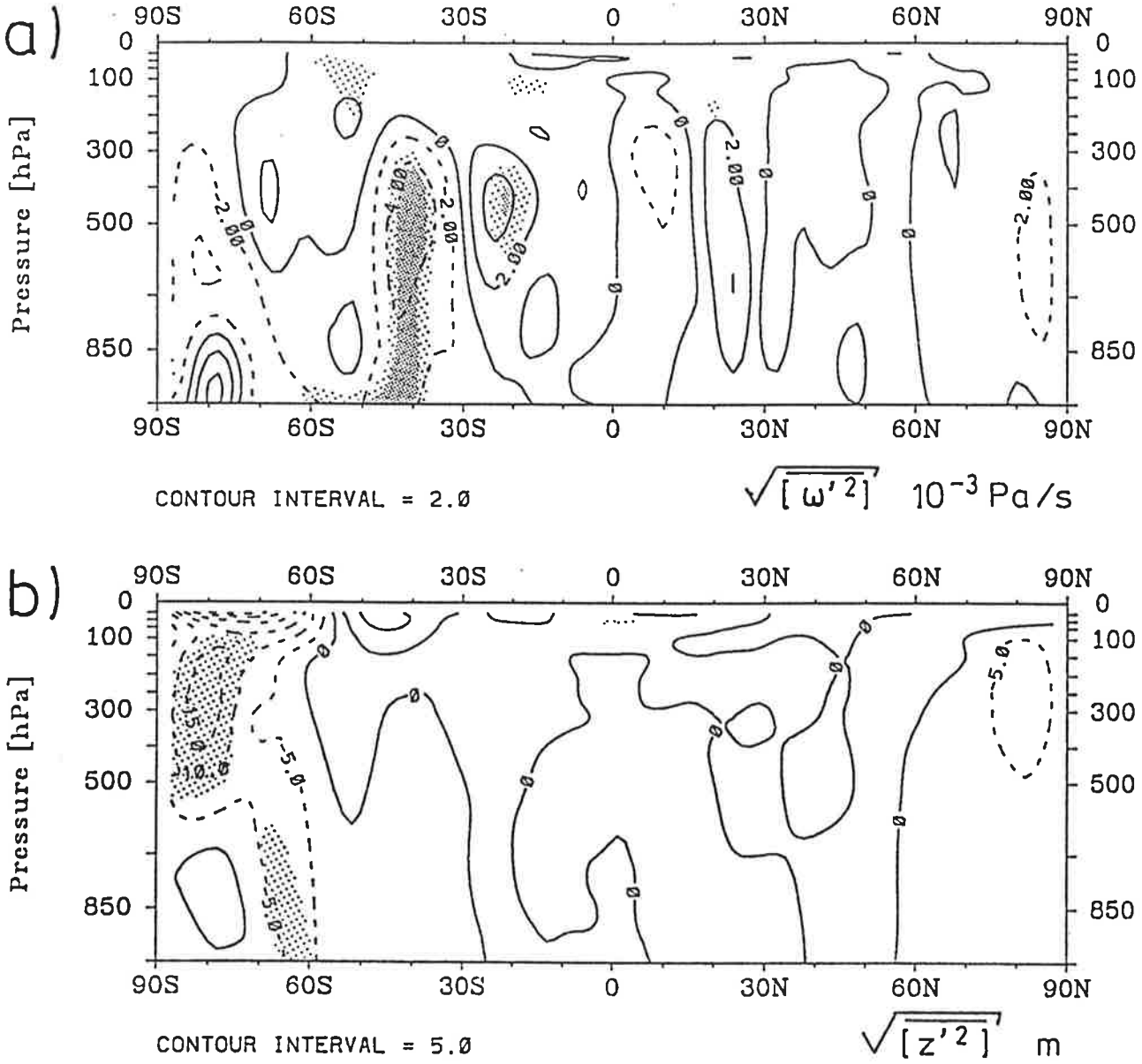

Figure 6

The latitude-height distribution of the difference "experiment - control" in the zonally averaged time-mean eddy fields of

a) the vertical ω-wind $(\overline{[\omega'^2]}^{1/2}$; units: 10^{-3} Pa/s)

b) the geopotential height $(\overline{[z'^2]}^{1/2}$; units: gpm)

Differences which are locally significant at the 5% (1%) level are indicated by light (heavy) shading.

Consistent with these results, an analysis of the 2-15 day band-pass filtered variance of geopotential height at 500 hPa yields reduced storminess over most of the Southern Hemisphere (not shown).

Zonally averaged surface fluxes

The surface momentum and latent heat flux have increased in the Southern Hemisphere storm track, whereas the surface sensible heat flux has hardly changed (Fig. 7). In the control experiment the mean surface stress is 100 to 200 mPa and the mean surface latent heat flux is -100 to -200 W/m^2 in the storm track. The relative changes amount to 5-10% , which is much smaller than what would result from a mere doubling of the neutral drag coefficient with the atmospheric circulation fixed.

c) Analysis of the atmospheric energy cycle

The atmospheric energy cycle (Lorenz, 1955; Saltzman, 1957) consists of four reservoirs (Fig. 8):

- AZ: the *zonal available potential energy*, determined by the zonally averaged meridional temperature contrasts,
- KZ: the *zonal mean kinetic energy*, dominated by the zonal jet streams,
- AE: the *eddy available potential energy*, determined by temperature contrasts along longitudes
- KE: the *eddy kinetic energy*, determined by the variations of wind speed along longitudes

The conversions between the four reservoirs are:

- CZ: from AZ to KZ, expressing rising of warm air and sinking of cold air due to the mean meridional circulation,
- CE: from AE to KE, like CZ but due to eddies,
- CA: from AZ to AE, predominantly due to meridional transport of sensible heat against the meridional temperature gradient,
- CK: from KE to KZ, due to meridional transport of momentum against the meridional gradient of the zonal wind.

Zonal available potential energy is generated by net radiational heating and latent heat release in the tropics and by net infrared cooling in higher latitudes. Condensational heating and longitudinal variations of radiational heating are sources of eddy available potential energy. Zonal and eddy kinetic energy are dissipated by (turbulent) friction. Unfortunately, these sources and sinks are not provided as model output.

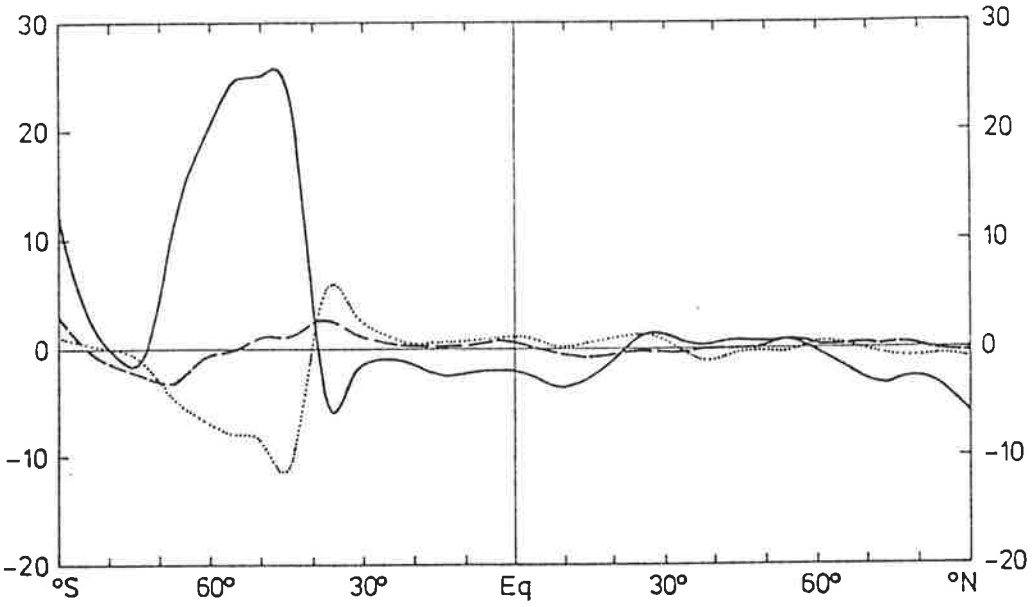

Figure 7

The difference "experiment - control" in the zonally averaged time-mean surface fluxes of momentum (solid, in mPa), sensible heat (dashed, in Wm^{-2}) and latent heat (dotted, in Wm^{-2}).

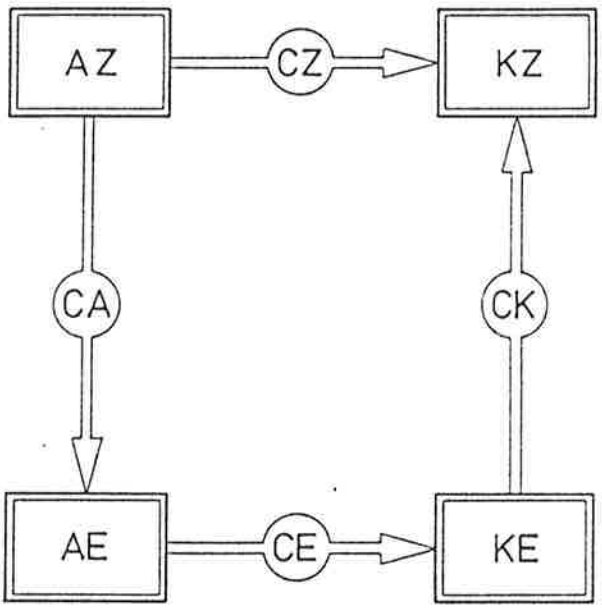

Figure 8

Schematic of the globally averaged atmospheric energy cycle. Arrows indicate the observed direction of the conversions.

The globally averaged terms of the atmospheric energy cycle are almost unaffected by the increase of the surface roughness. Therefore we do not discuss these. More insight is obtained from the latitude-height distributions of the conversions and reservoirs of the energy cycle.

Consistent with our previous findings, significant changes are limited to the Southern Hemisphere. The baroclinic conversions CA (not shown) and CE (Fig. 9a) as well as the reservoir AE (not shown) are reduced above the area with increased roughness and at the Antarctic coast. The poleward eddy momentum flux and the corresponding barotropic conversion CK have decreased in the upper troposphere (Fig. 9b). The reservoirs KZ and KE (eddy and zonal mean kinetic energy) are significantly reduced at all tropospheric levels between 30°S and 60°S (not shown), consistent with the changes in eddy and zonal mean wind speeds.

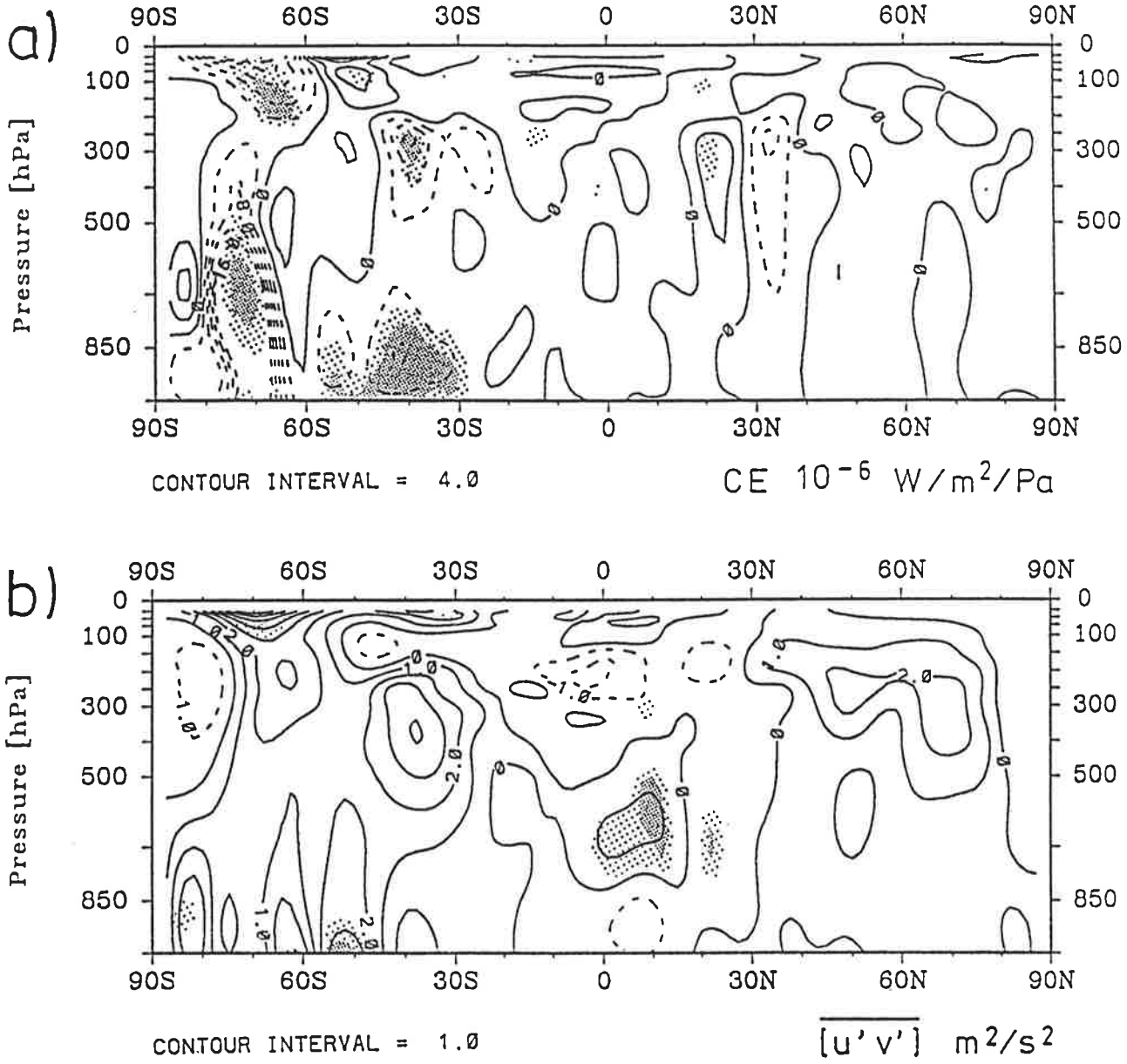

Figure 9

The latitude-height distribution of the difference "experiment - control" in the zonally averaged time-mean energy conversions:

a) CE (vertical eddy heat flux) from the reservoir AE (eddy available potential energy) to the reservoir KE (eddy kinetic energy) ($-R\ g^{-1}p^{-1}[\omega'T']$; units: 10^{-6} $Wm^{-2}Pa^{-1}$)

b) CK (eddy momentum flux) from the reservoir KE (eddy kinetic energy) to the reservoir KZ (zonal mean kinetic energy) ($[\overline{u'v'}]$; units: m^2s^{-2})

Differences which are locally significant at the 5% (1%) level are indicated by light (heavy) shading.

4. Discussion and Conclusions

a) Summary of the results

In our GCM experiments the enhancement of ocean surface roughness south of 40°S slows down the atmospheric circulation at all levels between 10°N and 70°S. This signal is globally significant. The largest impact is above the area of roughness enhancement, where both the zonal mean and the eddy activity has reduced. The meridional temperature gradient has not changed, but there is a shift of mass towards higher latitudes. At low levels the temperature has slightly increased, so that the static stability is slightly reduced. Transient eddy variance in the wind, the geopotential height and the temperature has decreased also.

b) Implications for the parameterization of ocean wave growth

We mentioned in the Introduction that our original motivation for the present study was to examine the effect that the growth of ocean waves might have on the atmospheric circulation. Since waves are generated by storms we enhanced the ocean surface roughness uniformly in the Southern Hemisphere storm track.

Parallel to this study, Weber et al. (1991) coupled a full ocean wave model (WAMDIG, 1988) to the ECHAM atmospheric GCM. They found that in the long-term mean ocean surface roughness was indeed fairly uniformly enhanced in the Southern Hemisphere storm track, but the enhancement (about 20%) was much weaker than assumed here. However, on a day-to-day basis the roughness enhancement showed complicated spatial and temporal patterns, reflecting the individual storms instead of the storm track. The mean meridional gradient of geopotential height had not *de*creased in the coupled wave-atmosphere experiment, as in the present experiment, but had *in*creased. Also, the eddy-activity had not *de*creased but had slightly *in*creased and had shifted somewhat to higher latitudes.

We conclude from these results that a uniform enhancement of the ocean surface roughness in the storm tracks is not an adequate parameterization of the impact which growing ocean waves have on the atmospheric circulation.

c) Discussion of the results

In order to understand the dynamic response of the tropospheric circulation to the increased ocean surface roughness z_o, we relate the enhancement of z_o step by step to the reduction of the zonal mean wind. The first effect of the enhanced roughness is to increase the surface latent heat flux, one of the sources for eddy available potential energy, and to increase the surface momentum flux, a sink for eddy and zonal mean kinetic energy.

The direct effect of the enhanced surface friction, a decrease of the low level circulation, is observed. The indirect effects are less obvious: the increased roughness affects the development of baroclinic eddies, which interact with the mean circulation.

Branscome et al. (1989) examined the nonlinear development of baroclinic waves. They found that increased surface heat fluxes and friction causes a reduction of the meridional eddy sensible heat flux in the lower troposphere and of the meridional eddy momentum flux in the upper troposphere, as well as reduced eddy energies. Similar signals in the meridional and vertical eddy sensible heat fluxes and in the eddy available potential energy are often found within the energy cycle (Ulbrich and Speth, 1991).

Using a linear quasi-geostrophic model Dethloff and Schmitz (1982) related anomalous meridional eddy momentum fluxes to anomalous zonal mean flow. They found that a weakened poleward eddy momentum flux at upper levels induces an easterly anomalous wind equatorward of the momentum flux forcing and a westerly anomalous wind poleward of it. The anomalous patterns of the tropospheric wind (Fig. 4a) and of the eddy momentum flux (Fig. 9b) in our GCM experiment are qualitatively consistent with Dethloff and Schmitz's findings (see their Figs. 5 and 2). Also the magnitude of the anomalies (1-3 ms^{-1} in wind speed and 3-4 m^2s^{-2} in momentum flux) agree with Dethloff and Schmitz's results.

We propose that the tropospheric response in our experiment is controlled by two coupled processes. One process is the direct impact of the zonally uniform enhanced roughness on the low-level zonal mean circulation. The other process consists of two steps. The increased roughness weakens the eddy fields and the meridional eddy momentum flux, which again weakens the mean zonal flow.

Acknowledgements

We thank the ECHAM group at the Meteorologisches Institut der Universität Hamburg for preparing thoroughly the GCM and offering it to the scientific community as a readily accessible community model. We are particularly grateful to Ulrich Schlese and Ulrich Cubasch who helped us to realize our experimental design. Peter Janssen gave valuable advice; Andreas Hense supplied us with his statistical software package. Marion Grunert, Doris Lewandowksi and Norbert Noreiks prepared the diagrams.

The project was in part financed by the EC through project EPOC 0003-C and by the BMFT through projects 07 KFT 306 and 07 KFT 012.